

# Freezing a Flock: Motility-Induced Phase Separation in Polar Active Liquids

Delphine Geyer,<sup>1</sup> David Martin,<sup>2</sup> Julien Tailleur,<sup>2</sup> and Denis Bartolo<sup>1</sup>

<sup>1</sup>*Univ. Lyon, ENS de Lyon, Univ. Claude Bernard,  
CNRS, Laboratoire de Physique, F-69342, Lyon, France*

<sup>2</sup>*Laboratoire Matière et Systèmes Complexes, UMR 7057 CNRS/P7, Université Paris Diderot,  
10 rue Alice Domon et Leonie Duquet, 75205 Paris cedex 13, France*

(Dated: March 5, 2019)

Combining model experiments and theory, we investigate the dense phases of polar active matter beyond the conventional flocking picture. We show that above a critical density flocks assembled from self-propelled colloids arrest their collective motion, lose their orientational order and form solids that actively rearrange their local structure while continuously melting and freezing at their boundaries. We establish that active solidification is a first-order dynamical transition: active solids nucleate, grow, and slowly coarsen until complete phase separation with the polar liquids they coexist with. We then theoretically elucidate this phase behaviour by introducing a minimal hydrodynamic description of dense polar flocks and show that the active solids originate from a Motility-Induced Phase Separation. We argue that the suppression of collective motion in the form of solid jams is a generic feature of flocks assembled from motile units that reduce their speed as density increases, a feature common to a broad class of active bodies, from synthetic colloids to living creatures.

## I. INTRODUCTION

The emergence of collective motion in groups of living creatures or synthetic motile units is now a well established physical process [1–6]: Self-propelled particles move coherently along the same direction whenever velocity-alignment interactions overcome orientational perturbations favoring isotropic random motion. This minimal picture goes back to Vicsek’s seminal work [7] and made it possible to elucidate the flocking dynamics of systems as diverse as bird groups, polymers surfing on motility assays, shaken grains, active colloidal fluids and drone fleets [6, 8–13]. From a theoretical perspective, flocks are described as flying ferromagnets where point-wise spins move at constant speed along their spin direction [1, 3, 7, 14, 15]. However, this simplified description is inapt to capture the dynamics of dense populations where contact interactions interfere with self-propulsion and ultimately arrest the particle dynamics. Until now, aside from rare theoretical exceptions [14, 16–19], the consequences of motility reduction in dense flocks has remained virtually uncharted despite its relevance to a spectrum of active bodies ranging from marching animals to robot fleets and active colloids.

In this article, combining quantitative experiments and theory, we investigate the suppression of collective motion in high-density flocks. We show and explain how polar assemblies of motile colloids turn into lively solid phases that actively rearrange their amorphous structure, but do not support any directed motion. We establish that active solidification of polar liquids is a first-order dynamical transition: active solids nucleate, grow, and slowly coarsen until complete phase separation. Even though they are mostly formed of particles at rest, we show that active solids steadily propagate through the polar liquids they coexist with. Using numerical simula-

tions and analytical theory, we elucidate all our experimental findings and demonstrate that the solidification of colloidal flocks provides a realization of the long sought-after complete Motility-Induced Phase Separation [5, 20–25].

## II. SOLIDIFICATION OF COLLOIDAL FLOCKS

Our experiments are based on colloidal rollers. In brief, taking advantage of the so-called Quincke instability [10, 26], we motorize inert colloidal beads and turn them into self-propelled rollers all moving at the same constant speed  $v_0 = 1040 \mu\text{m/s}$  when isolated, see also Appendix B. We observe  $5 \mu\text{m}$  colloidal rollers propelling and interacting in microfluidic racetracks of length  $L_0 = 9.8 \text{ cm}$  and width  $2 \text{ mm}$ , Fig. 1a. Both hydrodynamic and electrostatic interactions promote alignment of the roller velocities. As a result, the low-density phase behavior of the Quincke rollers falls in the universality class of the Vicsek model [7, 27–29]. At low packing fraction, Fig. 1b, they form an isotropic gas where the density  $\rho(\mathbf{r}, t)$  is homogeneous and the local particle current  $\mathbf{W}(\mathbf{r}, t)$  vanishes. Increasing the average packing fraction  $\rho_0$  above  $\rho_F = 0.02$ , Fig. 1c, the rollers undergo a flocking transition. The transition is first-order, and polar liquid bands, where all colloids propel on average along the same direction, coexist with an isotropic gas [10, 30]. Further increasing  $\rho_0$ , the ordered phase fills the entire system and forms a homogeneous polar liquid which flows steadily and uniformly as illustrated in Supplementary Movie 1. In polar liquids both  $\mathbf{W}(\mathbf{r}, t)$  and  $\rho(\mathbf{r}, t)$  display small (yet anomalous) fluctuations, and orientational order almost saturates, see Fig. 1d and [31]. This low-density behavior provides a prototypical example of flocking physics.

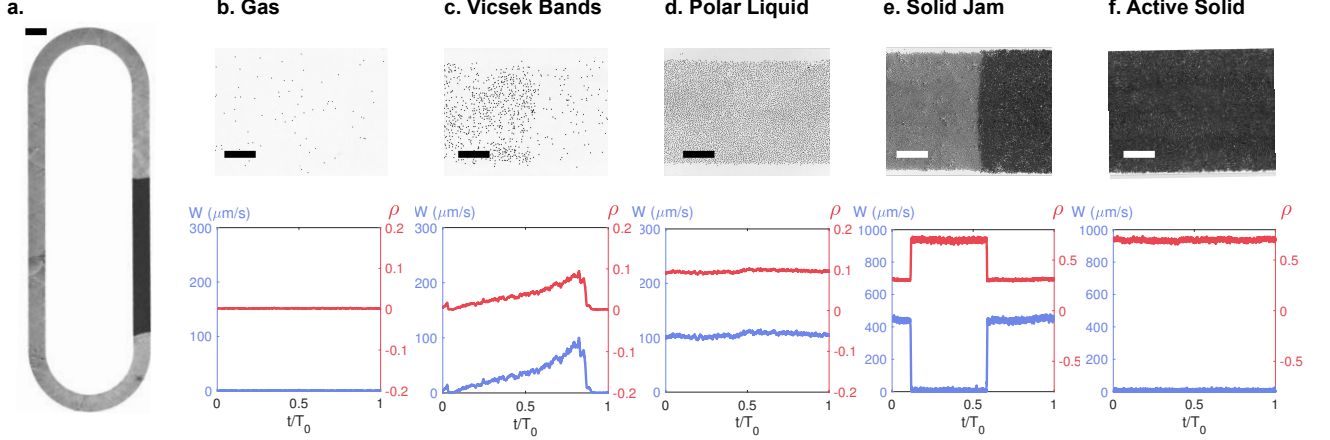


FIG. 1. **The dynamical phases of Quincke rollers.** **a.** Picture of a microfluidic racetrack where  $\sim 3 \times 10^6$  Quincke rollers interact. An active solid (dark grey) propagates through a polar liquid (light grey). Scale bar: 2 mm. **b–f.** Top panel: close-up pictures of Quincke rollers in the racetrack. Scale bars:  $250 \mu\text{m}$ . Bottom panel: longitudinal component of the particle current  $W$  and density plotted as a function of a normalized time. Both  $W$  and  $\rho$  are averaged over an observation window of size  $56 \mu\text{m} \times 1120 \mu\text{m}$ .  $T_0$  is arbitrarily chosen to be the time taken by an active solid to circle around the race track. **b.** Gas phase ( $\rho_0 = 0.002$ ). The density is homogeneous and the system does not support any net particle current. **c.** Coexistence between an active gas and a denser polar band ( $\rho_0 = 0.033$ ). A heterogeneous polar-liquid drop propagates at constant speed through a homogeneous isotropic gas in the form of a so-called Vicsek band. **d.** Polar-liquid phase ( $\rho_0 = 0.096$ ). The homogeneous active fluid supports a net flow. **e.** Coexistence between a polar liquid and an amorphous active solid ( $\rho_0 = 0.49$ ). The high-density solid is homogeneous but, unlike the polar liquid, does not support any net particle current. **f.** Homogeneous active solid phase ( $\rho_0 = 0.70$ ).

However, when  $\rho_0$  exceeds  $\rho_S \simeq 0.55$  collective motion is locally suppressed and flocking physics fails in explaining our experimental observations. Particles stop their collective motion and jam as exemplified in Supplementary Movies 2 and 3. The jams are active solids that continuously melt at one end while growing at the other end. This lively dynamics hence preserves the shape and length ( $L_S$ ) of the solid which propagates at constant speed upstream the polar-liquid flow, see the kymograph of Fig. 2a. Further increasing  $\rho_0$ , the solid region grows and eventually spans the entire system, Fig. 1f.

Active solids form an amorphous phase. The pair correlation function shown in Figs. 2b and 2c indicate that active solids are more spatially ordered than the polar liquid they coexist with, but do not display any sign of long-range translational order. As clearly seen in Supplementary Movie 2, the colloid dynamics are however markedly different in the two phases. While they continuously move at constant speed in the polar liquid, in the active solid, the rollers spend most of their time at rest thereby suppressing any form of collective motion and orientational order, Figs. 2d and 2e.

We stress that the onset of active solidification corresponds to an area fraction  $\rho_S \simeq 0.5$  which is much smaller than the random close packing limit ( $\rho_0 = 0.84$ ) and than the crystallization point of self-propelled hard disks reported by Briand and Dauchot ( $\rho_0 \sim 0.7$ ) in [32]. This marked difference hints towards different physics which

we characterize and elucidate below.

### III. THE EMERGENCE OF AMORPHOUS ACTIVE SOLIDS IS A FIRST-ORDER PHASE SEPARATION

We now establish that the formation of active solids occurs according to a first order phase-separation scenario. Firstly, Figs. 3a and b indicate that, upon increasing  $\rho_0$ , the extent of the solid phase has a lower bound: starting from a homogeneous polar liquid, the solid length  $L_S$  discontinuously jumps to a finite value before increasing linearly with  $\rho_0 - \rho_L^b$ , where  $\rho_L^b = 0.53$ , see Fig. 3b. The smallest solid observed in a stationary state is as large as  $L_S \sim 1.4\text{cm}$ . Smaller transient solid jams do form at local heterogeneities, but they merely propagate over a finite distance before rapidly melting, see Supplementary Movie 4. This observation suggests the existence of a critical nucleation radius for the solid phase.

Secondly, while the packing fraction of a polar liquid obviously increases with  $\rho_0$ , its value saturates as it coexists with an active solid, Fig. 3c. At coexistence, the local densities in the bulk of the liquid and solid phases are independent of the average density  $\rho_0$ :  $\rho_S^b = 0.77$  and  $\rho_L^b = 0.53$ , which again supports a nucleation and growth scenario. Increasing  $\rho_0$  leaves the inner structure of both phases unchanged and solely increases the frac-

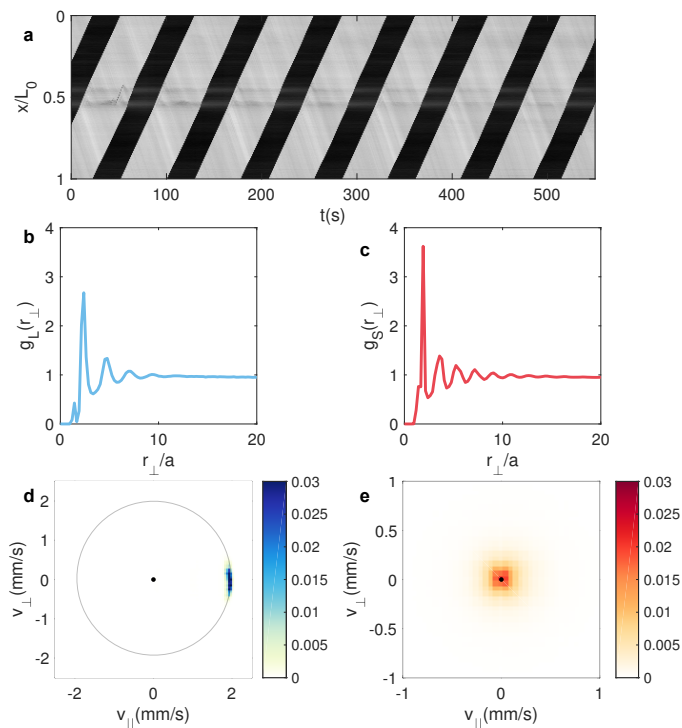


FIG. 2. **Structure and dynamics of active jams.** **a.** The kymograph of the measured light intensity averaged over the racetrack width shows how an active solid (dark region) propagates at constant speed through a homogeneous polar liquid (light region). **b** and **c.** Pair-correlation functions measured in the polar liquid ( $g_L$ ) and in the coexisting active-solid phase ( $g_S$ ).  $\rho_0 = 0.58$ . Both pair-correlation functions are plotted versus the interparticle distance  $r_\perp$  in the direction transverse to the mean polar-liquid flow.  $g_S$  displays more peaks than  $g_L$  revealing a more ordered structure, but translational order merely persists over a few particle diameters. **d.** Probability density functions of the roller velocities in the polar liquid region. The distribution is peaked around  $\nu_0 \hat{x}_\parallel$ , where  $\hat{x}_\parallel$  is the vector tangent to the racetrack centerline. **e.** Probability density functions of the roller velocities in the active jam region. The distribution is peaked around 0. The rollers remain mostly at rest. **b, c, d,** and **e:** average area fraction  $\rho_0 = 0.58$ .

tion of solid  $L_S/L_0$  in the racetrack. We find that, as in equilibrium phase separation, the length of the solid region is accurately predicted using a lever rule constructed from the stationary bulk densities  $\rho_S^b$  and  $\rho_L^b$ , see Fig. 3b.

Thirdly, we stress that when multiple jams nucleate in the device, they propagate nearly at the same speed, see Supplementary Movie 4. Therefore, they cannot catch up and coalesce. The system in fact reaches a stationary state thanks to a slow coarsening dynamics illustrated in Fig. 3d where we show the temporal evolution of the length of two macroscopic active solids (red symbols) and of the overall solid fraction (dark line). One solid jam grows at the expense of the other and coarsening operates leaving the overall fraction of solid constant. All of our

experiments end with complete phase separation: a single macroscopic active solid coexists with a single active liquid phase. The final state of the system is therefore uniquely determined by two macroscopic control parameters: the average density  $\rho_0$  and the magnitude  $E_0$  of the electric field used to power the rollers.

Finally, the most compelling argument in favour of a genuine first-order phase separation is the bistability of the two phases. Fig. 3b shows that at the onset of solidification, depending on the (uncontrolled) initial conditions, the system is either observed in a homogeneous polar liquid or at liquid-solid coexistence. The bistability of the active material is even better evidenced when cycling the magnitude of  $E_0$  (cycling the average density is not experimentally feasible). Fig. 3e shows the temporal variations of the active-solid fraction upon triangular modulation of  $E_0$ , see also Supplementary Movie 5. When  $E_0$  increases an active-solid nucleates and quickly grows. When  $E_0$  decreases, the solid continuously shrinks and eventually vanishes at a field value smaller than the nucleation point. The asymmetric dynamics of  $L_S/L_0$  demonstrates the existence of a metastable region in the phase diagram. As shown in Fig. 3f, the metastability of the active solid results in the hysteretic response of  $L_S$ , the hallmark of a first-order phase transition. We also note that the continuous interfacial melting observed when  $E_0$  smoothly decreases contrasts with the response to a rapid field quench, see Supplementary Movie 6. Starting with a stationary active solid, a rapid quench results in a destabilization of the solid bulk akin to a spinodal decomposition dynamics.

Altogether these measurements firmly establish that the emergence of active solids results from a first-order phase separation, which we theoretically elucidate below.

#### IV. MOTILITY-INDUCED PHASE SEPARATION IN HIGH-DENSITY POLAR FLOCKS

##### A. Nonlinear hydrodynamic theory

As a last experimental result, we show in Fig. 4a how the roller speed  $\nu_0(\rho)$  varies with the *local* density  $\rho(\mathbf{r}, t)$  evaluated in square regions of size  $12a \sim 29 \mu\text{m}$ . These measurements correspond to an experiment where a solid jam coexists with a homogeneous polar liquid.  $\nu_0(\rho)$  hardly varies at the smallest densities and sharply drops towards  $\nu_0(\rho) = 0$  when  $\rho(\mathbf{r}, t)$  exceeds  $\bar{\rho} \sim 0.35$ . Although we cannot positively identify the microscopic origin of this abrupt slowing down, we detail a possible explanation in Appendix A. Simply put, the lubrication interactions between nearby colloids with colinear polarizations result in the reduction of their rotation rate which ultimately vanishes at contact: near-field hydrodynamic interactions frustrate self-propulsion. Instead of elaborating a microscopic theory specific to colloidal rollers as

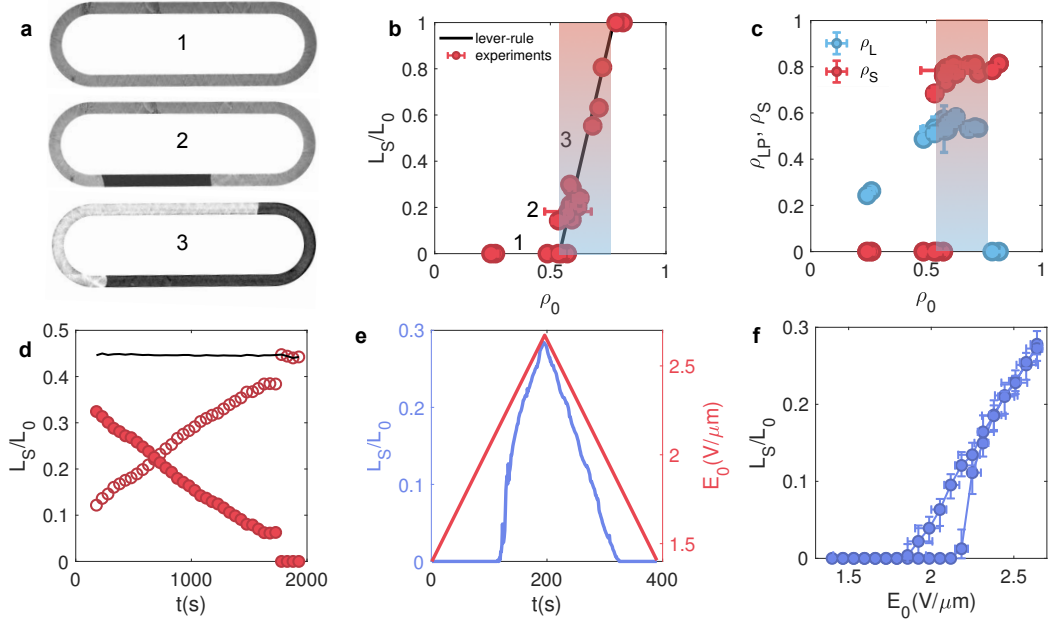


FIG. 3. **Active solidification is a first-order phase separation.** **a.** Solid jams in a racetrack at  $\rho_0 = 0.38, 0.58, 0.65$ . Increasing the average packing fraction, the extent of the active solid increases. **b.** Solid fraction plotted versus the average density  $\rho_0$ . Note the discontinuous jump and the two possible states at the onset of solidification. **c.** Density of the polar-liquid phase (blue circles) and of the active-solid phase (red circles) plotted versus  $\rho_0$ . In steady state, the liquid density increases with  $\rho_0$  until an active solid forms, the density in both phases then remains constant. In **b.** and **c.** the shaded regions indicate the coexistence between the polar liquid and an active solid phases. **d.** Coarsening dynamics. Two solid jams coexist only over a finite time period. The larger jam (filled symbols) shrinks and eventually vanishes in favor of the smaller one (open symbols). The total fraction of solid phase in the racetrack (black line) remains constant over time. **e.** Solid fraction (blue line) and magnitude of the electric field (red line) plotted versus time. Over a range of  $E_0$  values, the active-solid fraction is different when increasing or decreasing the electric field. **f.** The extent of the traffic jam follows a hysteresis loop when cycling the field amplitude.

in [10], we instead adopt a generic hydrodynamic description to account for all our experimental findings.

We start with a minimal version of the Toner-Tu equations which proved to correctly capture the coexistence of active gas and polar-liquid drops at the onset of collective motion [2, 33, 34]. For sake of simplicity we ignore fluctuations transverse to the mean-flow direction and write the hydrodynamic equations for the one-dimensional density  $\rho(x, t)$  and longitudinal current  $W(x, t)$ :

$$\partial_t \rho + \partial_x W = D_\rho \partial_{xx} \rho, \quad (1)$$

$$\begin{aligned} \partial_t W + \lambda W \partial_x W = D_W \partial_{xx} W - \partial_x [\epsilon_1(\rho) \rho] \\ + [\rho \epsilon_2(\rho) - \phi] W - a_4 W^3. \end{aligned} \quad (2)$$

We modify the Toner-Tu hydrodynamics to account for the slowing down of the rollers when  $\rho$  exceeds  $\bar{\rho}$ , Fig. 4a. Two terms must be modified to capture this additional physics: the so-called pressure term  $\rho \epsilon_1(\rho)$ , and the density-dependent alignment term  $\rho \epsilon_2(\rho)$  responsible for the emergence of orientational order and collective motion.

Coarse-graining microscopic flocking models typically leads to a pressure term proportional to the particle

speed [1, 28]. We therefore expect  $\epsilon_1(\rho)$  to sharply decrease when  $\rho(x, t) > \bar{\rho}$ . At even higher densities, we also expect the repulsion and contact interactions between the particles to result in a pressure increase with the particle density [10, 35]. We henceforth disregard this second regime which is not essential to the nucleation and propagation of active solids. The functional forms of  $\epsilon_2(\rho)$  is phenomenologically deduced from the loss of orientational order in the solid phase reported in Figs. 2e. This property is modelled by a function  $\epsilon_2(\rho)$  which decreases from a constant positive value in the low-density phases to a vanishing value deep in the solid phase. In all that follows, we conveniently assume  $\epsilon_2(\rho)$  and  $\epsilon_1(\rho)$  to be proportional. This assumption is supported by the similar variations observed for the roller speed and local current in Fig. 4a. In practice, we take  $\epsilon_i = \sigma_i [1 - \tanh((\rho - \bar{\rho})/\xi)]$ , where  $\sigma_1$  and  $\sigma_2$  are constant.

Numerical resolutions of Eqs. (1) and (2) at increasing densities faithfully account for the five successive phases observed in our experiments, see Fig. 4 and Appendix B. At low densities, we first observe the standard

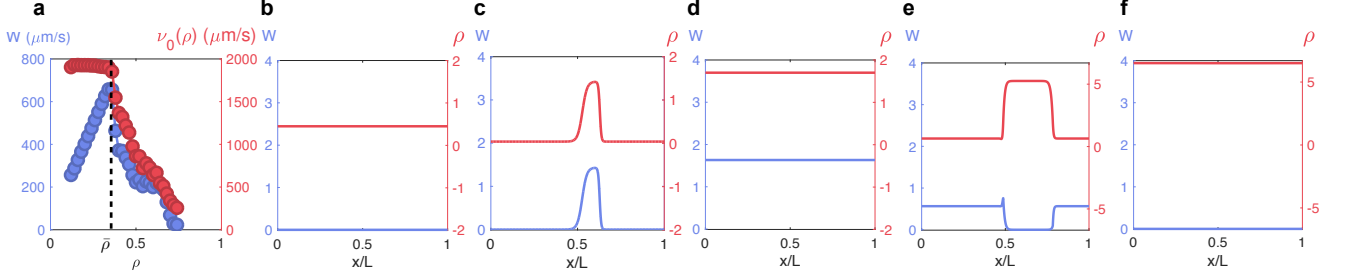


FIG. 4. **Nonlinear hydrodynamics of polar active matter.** **a.** Average velocity  $\nu_0(\mathbf{r}, t)$  of the colloids and local magnitude of the longitudinal current  $W(\mathbf{r}, t)$  plotted as a function of the local density  $\rho(\mathbf{r}, t)$ . **b-e.** Successive phases observed in the resolution of Eqs. (1) and (2) at increasing densities  $\rho = (0.10, 0.18, 1.7, 1.96, 6.5)$ . The position  $x$  is normalized by the system size  $L$ . Simulation parameters:  $D_\rho = 0.2$ ,  $D_W = 1$ ,  $\lambda = 1$ ,  $a_4 = 0.45$ ,  $\sigma_1 = 0.2$ ,  $\bar{\rho} = 2$ ,  $\xi = 0.01$ ,  $\sigma_2 = 1$ ,  $\phi = 0.5$ ,  $L = 200$ ,  $dx = 0.05$ ,  $dt = 0.005$ .

Vicsek transition: a disordered gas phase is separated from a homogeneous polar liquid phase by a coexistence region where ordered bands propagate through a disordered background [15]. This phase transition occurs at very low area fraction ( $\rho_0 \sim \phi \ll \bar{\rho}$ ), in a regime where the colloidal rollers experience no form of kinetic hindrance as they interact, therefore  $\epsilon_i(\rho) \simeq \sigma_i$ . In agreement with our experiments, a second transition leads to the coexistence between a polar liquid of constant density  $\rho_L^b$  and an apolar dense phase of constant density  $\rho_S^b$ . This jammed phase propagates backwards with respect to the flow of the polar liquid as does the active solids we observe in our experiments. This second transition shares all the signatures of the first-order phase separation reported in Fig. 3. Figs. 5a, 5b and 5c indicate that the jammed phase obeys a lever rule, its width increases linearly with  $\rho_0 - \rho_L^b$ , while the velocity  $c$  and the shape of the fronts remains unchanged upon increasing  $\rho_0$ . The first order nature of the transition is further supported by Supplementary Movie 7 which shows the existence of a hysteresis loop when ramping up and down the average density.

### B. Spinodal instability of polar liquids and domain wall propagation

Having established the predictive power of our hydrodynamic model, we now use it to gain physical insight into the origin of active solidification. We focus on the experimentally relevant situation where  $\bar{\rho} \gg \phi_g$ , i.e. where the slowing down of the particle occurs at area fractions much larger than the onset of collective motion. Given this hierarchy, at low densities, when  $\rho_0 \ll \bar{\rho}$ , the hydrodynamic equations Eqs. (1)-(2) correspond to that thoroughly studied in [33, 34, 36]. They correctly predict a first order transition from an isotropic gas to a polar-liquid phase, see also Appendix C.

The phase separation between a polar liquid and a jammed phase becomes also clear when performing a

linear stability analysis of the homogeneous solutions of Eqs. (1)-(2), see Appendix C where the stability of the various phases is carefully discussed. At high density, the stability of polar liquids where  $\rho = \rho_0$  and  $W = W_0 \neq 0$  is limited by a phenomenon that is not captured by classical flocking models. When  $\rho_0 \gg \phi + \epsilon_2/(2\lambda\epsilon_2 + 4a_4\epsilon_1)$ , polar liquids are stable with respect to the spinodal decomposition into Vicsek bands, however another instability sets in whenever  $\epsilon'_i(\rho_0)\rho_0 + \epsilon_i(\rho_0)$  is sufficiently large and negative, which occurs when  $\rho$  approaches  $\bar{\rho}$ . This instability is responsible for the formation of active-solid jams. We learn from the stability analysis that it ultimately relies on the decrease of the effective pressure with density in Eq. (2) as a result of the slowing down of the colloids in dense environments. This criterion is exactly analogous to the spinodal decomposition condition in MIPS physics: the formation of active-solid jams results from a complete motility induced phase separation [20].

### C. Discussion

Two comments are in order. Firstly, our results provide a novel microscopic mechanism leading to MIPS. In classical systems such as Active Brownian Particles, repulsive interactions and persistent motion conspire to reduce the local current when active particles undergo head-on collisions [21, 23, 24]. Here we show that this microscopic dynamics is however not necessary to observe phase separation and MIPS transitions solely rely on the reduction of the active particle current as density becomes sufficiently high, irrespective of its microscopic origin. In the case of colloidal rollers, particle indeed do not experience any frontal collision when an active solid nucleate in a polar liquid, phase separation is however made possible by the slowing down of their rolling motion.

Secondly, another marked difference with the dense phases of conventional MIPS system is the steady propagation of the active solids through the dilute polar liquid.



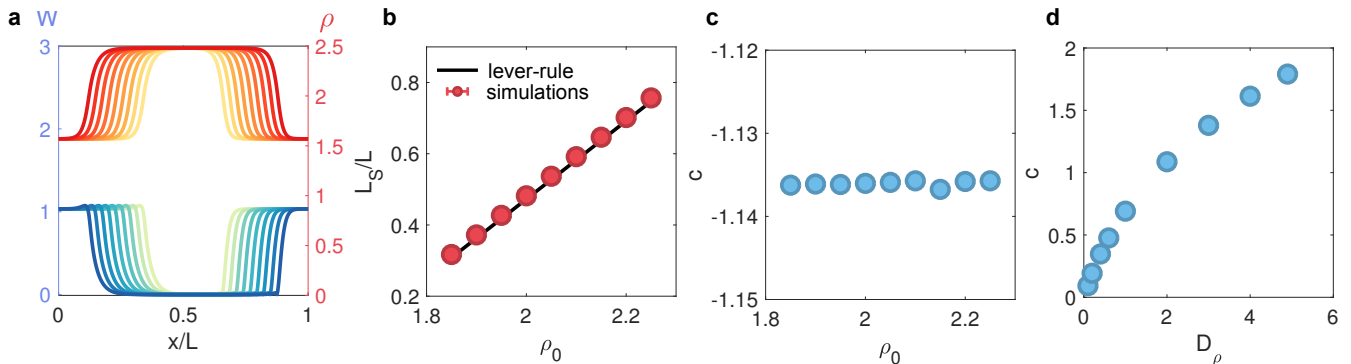


FIG. 5. **Shape and dynamics of active-solid jams.** **a.** Density and velocity profiles computed for different value of  $\rho_0$  : from 1.85 (light colors) to 2.25 (dark colors). Numerical resolution of Eqs. (1) and (2) with the hydrodynamic parameters:  $D_\rho = 5$ ,  $D_W = 10$ ,  $\lambda = 1$ ,  $a_4 = 1$ ,  $\sigma_1 = 1$ ,  $\bar{\rho} = 2$ ,  $\xi = 0.1$ ,  $\sigma_2 = 1$ ,  $\phi = 0.5$ ,  $L = 200$ ,  $dx = 0.01$ ,  $dt = 0.001$ . **b.** Length of the solid jam plotted versus  $\rho_0$  (symbols) and lever rule (solid line). Same parameters as in **a.** **c.** The speed of the solid jam  $c$  does not depend on the average density  $\rho_0$ . **d.** Variations of the propagation speed  $c$  as a function of the effective diffusivity  $D_\rho$ . Numerical parameters:  $D_W = 5$ ,  $\lambda = 1$ ,  $a_4 = 0.45$ ,  $\sigma_1 = 0.2$ ,  $\bar{\rho} = 2$ ,  $\xi = 0.01$ ,  $\sigma_2 = 1$ ,  $\phi = 0.5$ ,  $L = 200$ ,  $dx = 0.05$ ,  $dt = 0.005$ ,  $\rho_0 = 1.96$ .

This dynamics can be accounted for by our model. The two boundaries of the active solid are two domain walls that propagate at the same speed. The propagation of the domain wall at the front of the solid jam relies on a mechanism akin to actual traffic jam propagation: the directed motion of the particles incoming from the polar liquid cause an accumulation at the boundary with the arrested phase, in the direction opposing the spontaneous flow. By contrast, the propagation of the second domain wall, at the back of the solid jam, requires arrested particles to resume their motion. The formation of this smooth front originates from the mass diffusion terms in Eq. (1), which allows particles to escape the arrested solid phase and progressively resume their collective motion when reaching a region of sufficiently low density in the polar liquid. This diffusive spreading, however, does not rely on thermal diffusion. The roller diffusivity  $D_m \sim 10^{-13} \text{ m}^2/\text{s}$  is indeed negligible on the timescale of the experiments. Fortunately, other microscopic mechanisms, and in particular anisotropic interactions, lead to diffusive contributions to the density current [37]. A simple way to model this effect is to consider a velocity-density relation of the form  $v_0(\rho)[1 - r\mathbf{u} \cdot \nabla\rho]$  where  $\mathbf{u}$  is the orientation of the particle and  $r$ , which could be density dependent, quantifies the anisotropic slowing down of particles ascending density gradients. This anisotropic form is consistent with the polar symmetry of the flow and electric field induced by the Quincke rotation of the colloids. Coarse-graining the dynamics of self-propelled particles interacting via such a nonlocal quorum sensing rule was done in [37] and leads to an effective Fickian contribution  $\sim -\rho v_0 r \nabla\rho$  to the density current in Eq. (1). The ratio between the magnitude of this effective Fickian flux and that of thermal diffusion is readily estimated as  $(\rho v_0 r)/D_m \sim 10^5$ , assuming that  $r$  is of the order of the

a colloid diameter. Anisotropic interactions are therefore expected to strongly amplify the magnitude of  $D_\rho$ . In order to confirm the prominent role of this diffusion term in the active solid dynamics, we numerically measure the propagation speed  $c$  of the jammed region as a function of  $D_\rho$ . In agreement with the above discussion  $c$  is found to vanish as  $D_\rho \rightarrow 0$ , Fig. 5d thereby confirming the requirement of a finite diffusivity to observe stable active-solid jams. Simply put, the steady propagation of active solids relies on the balance between two distinct macroscopic phenomena: motility reduction at high density which results in the formation of sharp interfaces with the polar liquid, and the diffusive smoothing of the interfaces that enables particles trapped in the arrested solid phase to resume their motion by rejoining the polar-liquid flock.

## V. CONCLUSION

In summary, combining experiments on Quincke rollers and active-matter theory, we have shown that the phase behavior of polar active units is controlled by a series of two dynamical transitions: a Flocking transition that transforms active gases into spontaneously flowing liquids, and a Motility-Induced Phase Separation that results in the freezing of these polar fluids and the formation of active solids. Although most of their constituents are immobile, active solid jams steadily propagate through the active liquid they coexist with due to their continuous melting and freezing at their boundaries. Remarkably, Quincke rollers provide a rare example of an unhindered MIPS dynamics that is not bound to form only finite-size clusters, see [38] and references therein. Beyond the specifics of active rollers, we have

shown that the freezing of flocking motion and the emergence of active solids is a generic feature that solely relies on polar ordering and speed reduction in dense environments. A natural question to ask is whether suitably tailored polar and quorum-sensing interactions could yield ordered active solids. More generally understanding the inner structure and dynamic of active solids is an open challenge to active matter physicists.

## ACKNOWLEDGMENTS

D. G. and D. M. have equal contributions. We thank A. Morin for invaluable help with the experiments.

## Appendix A: Quincke rollers.

### 1. Motorization

Our experiments are based on colloidal rollers [10]. We motorize inert polystyrene colloids of radius  $a = 2.4 \mu\text{m}$  by taking advantage of the so-called Quincke electro-rotation instability [26, 39]. Applying a DC electric field to an insulating body immersed in a conducting fluid results in a surface-charge dipole  $\mathbf{P}$ . Increasing the magnitude of the electric field  $\mathbf{E}_0$  above the Quincke threshold  $E_Q$  destabilizes the dipole orientation, which in turn makes a finite angle with the electric field. A net electric torque  $\mathbf{T}_E \sim \mathbf{P} \times \mathbf{E}_0$  builds up and competes with a viscous frictional torque  $\mathbf{T}_V \sim \eta \boldsymbol{\Omega}$  where  $\boldsymbol{\Omega}$  is the colloid rotation rate and  $\eta$  is the fluid shear viscosity. In steady state, the two torques balance and the colloids rotate at constant angular velocity. As sketched in Fig. 6a and 6b, when the colloids are let to sediment on a flat electrode, rotation is readily converted into translation motion at constant speed  $v_0$  (in the direction opposite to the charge dipole). We stress that the direction of motion is randomly chosen and freely diffuses as a result of the spontaneous symmetry breaking of the surface-charge distribution.

### 2. Arresting Quincke rotation

We conjecture a possible microscopic mechanism to explain the arrest of the Quincke rotation at high area fraction: the frustration of rolling motion by lubrication interactions, Fig. 6c. The viscous torque  $\mathbf{T}_V$  acting on two nearby colloids rolling along the same direction is chiefly set by the lubricated flow in the contact region separating the two spheres.  $T_V$  therefore increases logarithmically with  $d - 2a$  where  $d$  is the interparticle distance [40]. As there exists an upper bound to the magnitude of the electric torque  $T_E$ , torque balance requires the rolling motion to become vanishingly slow as  $d - 2a$  goes to zero: lubricated contacts frustrate collective motion.

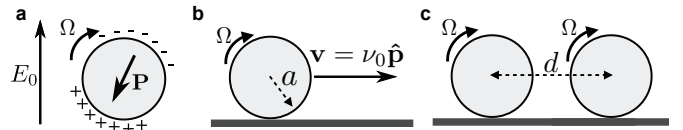


FIG. 6. **Quincke rollers.** **a.** When applying a DC electric field  $\mathbf{E}_0$  to an insulating sphere immersed in a conducting fluid, a charge dipole forms at the sphere surface. When  $E_0 > E_Q$ , the electric dipole makes a finite angle with the electric field causing the steady rotation of the sphere at constant angular speed  $\Omega$ . **b.** The rotation is converted into translation by letting the sphere to sediment on one electrode. When isolated, the resulting Quincke rotor rolls without sliding at constant speed:  $\nu_0(0) = a\Omega$ . **c.** When two colloids rolling in the same direction are close to each other the lubrication torque acting on the two spheres separated by a distance  $d$  scales as  $\ln d$  and hinders their rolling motion.

## Appendix B: Experimental and Numerical Methods

### 1. Experiments

The experimental setup is identical to that described in [31]. We disperse polystyrene colloids of radius  $a = 2.4 \mu\text{m}$  (Thermo Scientific G0500) in a solution of hexadecane including 0.055 wt% of AOT salt. We inject the solution in microfluidic chambers made of two electrodes spaced by a  $110 \mu\text{m}$ -thick scotch tape. The electrodes are glass slides, coated with indium tin oxide (Solems, ITOSOL30, thickness: 80 nm). We apply a DC electric field between the two electrodes ranging from  $1.3 \text{ V}/\mu\text{m}$  to  $2.6 \text{ V}/\mu\text{m}$  using a voltage amplifier. If not specified otherwise, the data correspond to experiments performed at  $1.8 \text{ V}/\mu\text{m}$ , i.e. at  $E_0/E_Q = 2$ . We confine the rollers inside racetrack by coating the bottom electrode with an insulating pattern preventing the electric current to flow outside of the racetrack. To do so, we apply  $2 \mu\text{m}$ -thick layer of insulating photoresist resin (Microposit S1818) and pattern it by means of conventional UV-Lithography as explained in [31].

In order to keep track of the individual-colloid position and velocity, we image the system with a Nikon AZ100 microscope with a 4.8X magnification and record videos with a CMOS camera (Basler Ace) at framerate up to 900 Hz. We use conventional techniques to detect and track all particles [41–43]. When performing large-scale observations we use a different setup composed of a 60 mm macro lens (Nikkor f/2.8G, Nikon) mounted on a 8 Mpxls, 14bit CCD camera (Prosilica GX3300).

### 2. Numerics

The numerical resolution of the Toner-Tu equations Eqs. (1) and (2) were done using a semi-spectral method with semi-implicit Euler scheme.

### Appendix C: Linear Stability of the generalized Toner-Tu equations

In this appendix we show how the succession of instabilities of the homogeneous solutions of Eqs. (1) and (2) correctly predict the full phase behavior observed in our experiments and numerical simulations.

#### 1. Stability of the disordered gas

We start by considering a homogeneous gas phase where  $\rho = \rho_0$ ,  $W = 0$ . The linearized dynamics of a small

perturbation  $\delta X \equiv (\delta\rho, \delta W)$  is given, in Fourier space, by  $\delta\dot{X}_k = M_k \delta X_k$ , where the dynamical matrix  $M_k$  is given by

$$M_k = \begin{pmatrix} -D_\rho k^2 & -ik \\ -(\epsilon_1 + \epsilon'_1 \rho_0)ik & (\rho_0 \epsilon_2 - \phi) - D_W k^2 \end{pmatrix} \quad (C1)$$

The eigenvalues  $\lambda_\pm$  of  $M_k$  determines the stability of the gas phase. We find:

$$\lambda_\pm = \frac{-(D_\rho k^2 + D_W k^2 - \rho_0 \epsilon_2 + \phi) \pm \sqrt{(D_\rho k^2 + D_W k^2 - \rho_0 \epsilon_2 + \phi)^2 - 4k^2(\epsilon_1 + \epsilon'_1) - 4(D_W k^2 - \rho_0 \epsilon_2 + \phi)D_\rho k^2}}{2} \quad (C2)$$

The gas is therefore unstable when either one of the following condition is satisfied:

$$\rho_0 \epsilon_2 - \phi > 0 \quad (C3)$$

$$(\epsilon_1 + \rho_0 \epsilon'_1) < -(D_W k^2 - \rho_0 \epsilon_2 + \phi)D_\rho \quad (C4)$$

The first condition is the standard spinodal instability leading to the emergence of collective motion and local orientational order [1, 36]. Beyond this classical results, we find a second instability akin to the MIPS criterion in the presence of translationnal diffusion [20]. This second condition arise from the decrease of the pressure term in Eq. (2) when  $\rho$  increases. This condition is not met in our experiments where we find that the emergence of polar order occurs before the onset of solidification.

#### 2. Stability of polar liquids

Let us now consider a polar liquid where  $\rho = \rho_0$ , and  $W = W_0$  with  $a_4 W_0^2 = (\rho_0 \epsilon_2 - \phi)$ . Following the same procedure as in the previous section, the linearized dynamics of a small perturbation  $\delta X = (\delta\rho, \delta W)$  is defined by the dynamical matrix:

$$M_k = \begin{pmatrix} M_{\rho\rho} & M_{\rho W} \\ M_{W\rho} & M_{WW} \end{pmatrix} \quad (C5)$$

where

$$M_{\rho\rho} = -D_\rho k^2, \quad (C6)$$

$$M_{\rho W} = -ik, \quad (C7)$$

$$M_{W\rho} = -(\epsilon_1 + \epsilon'_1 \rho_0)ik + (\epsilon_2 + \epsilon'_2 \rho_0)W_0 \quad (C8)$$

$$M_{WW} = (\rho_0 \epsilon_2 - \phi) - D_W k^2 - \lambda ik W_0 - 3a_4 W_0^2 \quad (C9)$$

Looking for the condition under which an eigenvalue admits a positive real part, so that the homogeneous solution becomes unstable, leads to:

$$-\alpha_6 k^6 - \alpha_4 k^4 - \alpha_2 k^2 - \alpha_0 > 0 \quad (C10)$$

with

$$\alpha_6 = D_W D_\rho (D_\rho + D_W) / W_0^2 \quad (C11)$$

$$\alpha_4 = \lambda^2 D_\rho D_W + 2D_\rho D_W (D_\rho + D_W) 2a_4 W_0^2 + (D_\rho + D_W)^2 [D_\rho 2a_4 + (\epsilon_1 + \epsilon'_1 \rho_0) / W_0^2] \quad (C12)$$

$$\alpha_2 = [D_\rho 2a_4 + [(D_\rho + D_W) (\rho_0 \epsilon'_2 + \epsilon_2)] + 2(D_\rho + D_W) 2a_4 (D_\rho 2a_4 W_0^2 + (\rho_0 \epsilon'_1 + \epsilon_1)) + D_\rho D_W (2a_4 W_0)^2 - 2\lambda D_\rho (\rho_0 \epsilon'_2 + \epsilon_2) \quad (C13)$$

$$\alpha_0 = (2a_4)^2 [D_\rho 2a_4 W_0^2 + (\rho_0 \epsilon'_1 + \epsilon_1)] + (\rho_0 \epsilon'_2 + \epsilon_2) 2a_4 W_0^2 - (\rho_0 \epsilon'_2 + W_0 \epsilon_2)^2 \quad (C14)$$

The analysis of the polynomial equation Eq.(C10) leads to a cumbersome instability criterion, that however simplifies in the context of our experiments where  $\phi \ll \bar{\rho}$ .

At low density,  $\rho_0 \ll \bar{\rho}$ , so that  $\rho_0 \epsilon'_1 + \epsilon_1 = \sigma_1$  and  $\rho_0 \epsilon'_2 + \epsilon_2 = \sigma_2$ , and only the constant term  $\alpha_0$  can be positive, which yields a simplified instability criterion:

$$\sigma_2 / (\sigma_2 \rho_0 - \phi) > 8a_4 D_\rho (\sigma_2 \rho_0 - \phi) + 4a_4 \sigma_1 + 2\lambda \sigma_2 \quad (C15)$$

In the limit of small  $D_\rho$ , relevant for our experiments [31], one recovers the spinodal instability criterion of a homogeneous polar liquid [34]

$$\phi + \frac{\sigma_2}{2\lambda \sigma_2 + 4a_4 \sigma_1} \gtrsim \sigma_2 \rho_0 \quad (C16)$$

For larger densities, deep in the polar-liquid phase when  $\rho_0 \sim \bar{\rho}$ , the instability criterion (C16) cannot be



satisfied. However,  $\epsilon'_i(\rho_0)$  is not negligible anymore, and a novel instability dictates the dynamics. All the  $\alpha_0$ ,  $\alpha_2$  and  $\alpha_4$  terms can be negative when  $\epsilon'_i\rho_0 + \epsilon_i$  is sufficiently large and negative (provided that  $D_W > D_\rho$ , which holds in our experimental conditions [31]). Again, one recovers a standard MIPS instability, which occurs in the vicinity of  $\bar{\rho}$  provided that the decrease of  $\epsilon_i(\rho)$  is sharp enough. We note that  $\alpha_0$  could also change and become negative for  $\epsilon'_i\rho_0 + \epsilon_i$  sufficiently large and positive. This situation is however not relevant for our experimental system but hints towards a possible additional instability of the ordered polar liquid, which will be discussed elsewhere.

#### Appendix D: Description of the Movies

*a. Movie 1.* Movie 1 shows a polar liquid flowing along a microfluidic racetrack. Dimensions of the observation window:  $1.3\text{mm} \times 1.3\text{mm}$ . The movie is slowed down by a factor 3.8.

*b. Movie 2.* Movie 2 Close-up in the microfluidic racetrack. We first see the polar liquid phase and then the compact active solid forming at one end and melting at the other end. Dimensions of the observation window:  $1.3\text{mm} \times 1.3\text{mm}$ . wide. The movie is slowed down by a factor 3.8.

*c. Movie 3.* Movie 3 shows a typical experiment in a racetrack where an active solid steadily propagate through the homogenous polar liquid it coexists with. The movie is sped up by a factor 30.

*d. Movie 4.* Movie 4 shows the coarsening dynamics of multiple active solids. The movie is sped up by a factor 30.

*e. Movie 5.* Hysteresis dynamics upon cycling the magnitude of the electric-field. This movie correspond to the experiments of Figs. 3e and 3f in the main document. The movie is sped up by a factor 30.

*f. Movie 6.* Response to an electric-field quench The bulk of the active solid is destabilized at all scales. This phenomenon is reminiscent to a spinodal decomposition scenario. The movie is sped up by a factor 30.

*g. Movie 7.* Numerical simulations of Eqs (1-2) with the same parameters as in Fig 5a-c, but with  $dx = 0.1$  and  $dt = 0.01$  to access longer time scales. Cycling the density  $\rho_0$  up and down shows a clear hysteresis loop. The polar liquid is stable up to a spinodal density  $\rho_L^s$ . After an initial instability, the coarsening process leads the system towards phase separation between a polar liquid at  $\rho_L^b$  and a solid phase, which is propagating backward. When decreasing the density, the solid jam is seen down to  $\rho_0 \simeq \rho_L^b \ll \rho_L^s$  highlighting the hysteresis loop.

- 
- [1] M. C. Marchetti, J. F. Joanny, S. Ramaswamy, T. B. Liverpool, J. Prost, Madan Rao, and R. Aditi Simha, “Hydrodynamics of soft active matter,” *Rev. Mod. Phys.* **85**, 1143–1189 (2013).
  - [2] John Toner, Yuhai Tu, and Sriram Ramaswamy, “Hydrodynamics and phases of flocks,” *Annals of Physics* **318**, 170 – 244 (2005), special Issue.
  - [3] Tamás Vicsek and Anna Zafeiris, “Collective motion,” *Physics reports* **517**, 71–140 (2012).
  - [4] Andrea Cavagna and Irene Giardina, “Bird flocks as condensed matter,” *Annual Review of Condensed Matter Physics* **5**, 183–207 (2014).
  - [5] Andreas Zöttl and Holger Stark, “Emergent behavior in active colloids,” *Journal of Physics: Condensed Matter* **28**, 253001 (2016).
  - [6] Qian Chen, Sung Chul Bae, and Steve Granick, “Directed self-assembly of a colloidal kagome lattice,” *Nature* **469**, 381 (2011).
  - [7] Tamás Vicsek, András Czirók, Eshel Ben-Jacob, Inon Cohen, and Ofer Shochet, “Novel type of phase transition in a system of self-driven particles,” *Physical review letters* **75**, 1226 (1995).
  - [8] Volker Schaller, Christoph Weber, Christine Semmrich, Erwin Frey, and Andreas R Bausch, “Polar patterns of driven filaments,” *Nature* **467**, 73 (2010).
  - [9] Yutaka Sumino, Ken H Nagai, Yuji Shitaka, Dan Tanaka, Kenichi Yoshikawa, Hugues Chaté, and Kazuhiro Oiwa, “Large-scale vortex lattice emerging from collectively moving microtubules,” *Nature* **483**, 448 (2012).
  - [10] Antoine Bricard, Jean-Baptiste Caussin, Nicolas Desreumaux, Olivier Dauchot, and Denis Bartolo, “Emergence of macroscopic directed motion in populations of motile colloids,” *Nature* **503** (2013).
  - [11] Julien Deseigne, Olivier Dauchot, and Hugues Chaté, “Collective motion of vibrated polar disks,” *Phys. Rev. Lett.* **105**, 098001 (2010).
  - [12] Nitin Kumar, Harsh Soni, Sriram Ramaswamy, and AK Sood, “Flocking at a distance in active granular matter,” *Nature Communications* **5** (2014).
  - [13] Gábor Vásárhelyi, Csaba Virág, Gergő Somorjai, Tamás Nepusz, Agoston E Eiben, and Tamás Vicsek, “Optimized flocking of autonomous drones in confined environments,” *Science Robotics* **3**, eaat3536 (2018).
  - [14] FDC Farrell, MC Marchetti, D Marenduzzo, and J Tailleur, “Pattern formation in self-propelled particles with density-dependent motility,” *Physical review letters* **108**, 248101 (2012).
  - [15] Guillaume Grégoire and Hugues Chaté, “Onset of collective and cohesive motion,” *Physical review letters* **92**, 025702 (2004).
  - [16] Fernando Peruani, Tobias Klaus, Andreas Deutsch, and Anja Voss-Boehme, “Traffic jams, gliders, and bands in the quest for collective motion of self-propelled particles,” *Physical Review Letters* **106**, 128101 (2011).
  - [17] Fernando Peruani and Markus Baer, “A kinetic model and scaling properties of non-equilibrium clustering of self-propelled particles,” *New Journal of Physics* **15**, 065009 (2013).
  - [18] David Nesbitt, Gunnar Pruessner, and Chiu Fan Lee, “Using a lattice boltzmann method to uncover novel phase transitions in dry polar active fluids,” *arXiv preprint arXiv:1902.00530* (2019).

- [19] Elena Sese-Sansa, Ignacio Pagonabarraga, and Demian Levis, “Velocity alignment promotes motility-induced phase separation,” *EPL (Europhysics Letters)* **124**, 30004 (2018).
- [20] Michael E Cates and Julien Tailleur, “Motility-induced phase separation,” *Annu. Rev. Condens. Matter Phys.* **6**, 219–244 (2015).
- [21] Yaouen Fily and M Cristina Marchetti, “Athermal phase separation of self-propelled particles with no alignment,” *Physical review letters* **108**, 235702 (2012).
- [22] Ivo Buttinoni, Julian Bialké, Felix Kümmel, Hartmut Löwen, Clemens Bechinger, and Thomas Speck, “Dynamical clustering and phase separation in suspensions of self-propelled colloidal particles,” *Physical review letters* **110**, 238301 (2013).
- [23] Gabriel S Redner, Michael F Hagan, and Aparna Baskaran, “Structure and dynamics of a phase-separating active colloidal fluid,” *Physical review letters* **110**, 055701 (2013).
- [24] Julian Bialké, Hartmut Löwen, and Thomas Speck, “Microscopic theory for the phase separation of self-propelled repulsive disks,” *EPL (Europhysics Letters)* **103**, 30008 (2013).
- [25] Guannan Liu, Adam Patch, Fatmagul Bahar, David Yllanes, Roy D Welch, M Cristina Marchetti, Shashi Thutupalli, and Joshua W Shaevitz, “A motility-induced phase transition drives myxococcus xanthus aggregation,” *arXiv preprint arXiv:1709.06012* (2017).
- [26] G. Quincke, “Über rotationen im constanten electrischen felde,” *Annalen der Physik*, 417–486 (1896).
- [27] Hugues Chaté, Francesco Ginelli, Guillaume Grégoire, and Franck Raynaud, “Collective motion of self-propelled particles interacting without cohesion,” *Physical Review E* **77**, 046113 (2008).
- [28] Eric Bertin, Michel Droz, and Guillaume Grégoire, “Hydrodynamic equations for self-propelled particles: microscopic derivation and stability analysis,” *Journal of Physics A: Mathematical and Theoretical* **42**, 445001 (2009).
- [29] Alexandre P Solon, Hugues Chaté, and Julien Tailleur, “From phase to microphase separation in flocking models: The essential role of nonequilibrium fluctuations,” *Physical review letters* **114**, 068101 (2015).
- [30] Alexandre Morin, Nicolas Desreumaux, Jean-Baptiste Caussin, and Denis Bartolo, “Distortion and destruction of colloidal flocks in disordered environments,” *Nature Physics* **1**, 1–6 (2016).
- [31] Delphine Geyer, Alexandre Morin, and Denis Bartolo, “Sounds and hydrodynamics of polar active fluids,” *Nature materials* **17**, 789 (2018).
- [32] G Briand and Olivier Dauchot, “Crystallization of self-propelled hard discs,” *Physical review letters* **117**, 098004 (2016).
- [33] Jean-Baptiste Caussin, Alexandre Solon, Anton Peshkov, Hugues Chaté, Thierry Dauxois, Julien Tailleur, Vincenzo Vitelli, and Denis Bartolo, “Emergent spatial structures in flocking models: a dynamical system insight,” *Physical review letters* **112**, 148102 (2014).
- [34] Alexandre P Solon, Jean-Baptiste Caussin, Denis Bartolo, Hugues Chaté, and Julien Tailleur, “Pattern formation in flocking models: A hydrodynamic description,” *Physical Review E* **92**, 062111 (2015).
- [35] Alexandre P Solon, Joakim Stenhammar, Raphael Witkowski, Mehran Kardar, Yariv Kafri, Michael E Cates, and Julien Tailleur, “Pressure and phase equilibria in interacting active brownian spheres,” *Physical review letters* **114**, 198301 (2015).
- [36] Shradha Mishra, Aparna Baskaran, and M. Cristina Marchetti, “Fluctuations and pattern formation in self-propelled particles,” *Phys. Rev. E* **81**, 061916 (2010).
- [37] Alexandre P Solon, ME Cates, and Julien Tailleur, “Active brownian particles and run-and-tumble particles: A comparative study,” *The European Physical Journal Special Topics* **224**, 1231–1262 (2015).
- [38] Elsen Tjhung, Cesare Nardini, and Michael E. Cates, “Cluster phases and bubbly phase separation in active fluids: Reversal of the ostwald process,” *Phys. Rev. X* **8**, 031080 (2018).
- [39] J. R. Melcher and G. I. Taylor, “Electrohydrodynamics: A review of the role of interfacial shear stresses,” *Annual Review of Fluid Mechanics* **1**, 111–146 (1969).
- [40] Sangtae Kim and Seppo J Karrila, *Microhydrodynamics: principles and selected applications* (Courier Corporation, 2013).
- [41] John C Crocker and David G Grier, “Methods of digital video microscopy for colloidal studies,” *Journal of colloid and interface science* **179**, 298–310 (1996).
- [42] Peter J Lu, Peter A Sims, Hidekazu Oki, James B Macarthur, and David A Weitz, “Target-locking acquisition with real-time confocal (tarc) microscopy,” *Optics express* **15**, 8702–8712 (2007).
- [43] D. Blair and E. Dufresne, “The matlab particle tracking code repository, retrieved from,” .